# Evolution of the bump-on-tail instability in compressing plasma

P. F. S C H M I T[1], C. R. M O O N E Y[1], I. Y. D O D I N[2]
and N. J. F I S C H[1]

[1]Princeton Plasma Physics Laboratory, Princeton University, Princeton, NJ 08543, USA
[2]Department of Astrophysical Sciences, Princeton University, Princeton, NJ 08544, USA

**Abstract.** Through particle-in-cell simulations, the evolution of the bump-on-tail instability (BoTI) is studied for plasma subject to one-dimensional mechanical compression. It is shown that the final state of BoTI differs from that described by quasilinear theory for stationary bulk plasma and can depend on the compression history. The transformation of thermal energy into wave energy increases the plasma compressibility, thereby decreasing the amount of mechanical work required to compress the plasma to a specified size. Also, the energy spectrum of the excited modes can be tailored by choosing a particular compression scenario, offering a new technique for manipulating plasmas mechanically.

## 1. Introduction

Compressing and expanding plasmas can be found throughout nature and the laboratory. In particular, experimental techniques for compressing plasmas for the purpose of inertial confinement fusion and high-energy density physics employ a number of different approaches, including laser implosion [1], magnetized liner implosion [2], and Z-pinches [3]. The physics of waves embedded in the targets is generally not considered. However, it has been recently suggested that seeding waves in such targets could yield new ways of manipulating plasmas. In particular, waves might be amplified adiabatically through compression [4] and then damp resonantly on a particular species in a switch-like manner [5], shaping selectively the tail distribution as prescribed.

This paper studies a particular aspect of such manipulations, namely, how the well-known bump-on-tail instability (BoTI) develops and saturates in compressing plasma. The quasilinear theory predicts a unique final state for a stationary (non-compressing) plasma exhibiting the instability, assuming the wave is sufficiently weak [6]. However, it is shown here that in compressing plasma with embedded waves the internal energy is no longer a state variable (that is, a function of volume only), but rather depends on the compression history. This effect is demonstrated numerically through particle-in-cell (PIC) simulations.

Specifically, the paper is organized as follows. In Sec. 2, the basic theory of BoTI in plasma under mechanical compression is discussed. Section 3 presents the results of the PIC simulations, illustrating the time history of BoTI in compressing plasma, including the evolution of the electron distribution function and the energy content and phase velocities of the excited modes. Section 4 describes how waves reduce

the amount of work required to compress a plasma and arrives at the fundamental result that energy is not necessarily a state variable for plasmas containing waves. Section 5 compares BoTI in one-dimensional (1D) compressing plasma with other variations of BoTI. Finally, Sec. 6 summarizes the main results of this paper.

## 2. Basic theory

In the presence of a small bump on the tail of the electron velocity distribution, the waves that are destabilized are small-amplitude, linear plasma oscillations, or Langmuir waves [6, 7], whose dispersion relation is given by

$$\omega = \omega_p \left( 1 + \frac{3}{2} \kappa^2 \right), \tag{2.1}$$

where $\omega_p$ is the electron plasma frequency, $\kappa = k\lambda_D$, $k$ is the wavenumber, $\lambda_D = v_T/\omega_p$ is the Debye length, $v_T = \sqrt{T/m_e}$ is the electron thermal velocity, $T$ is the electron temperature unperturbed by the waves, and $m_e$ is the electron mass. Equation (2.1) is asymptotically precise in the fluid limit at small but non-zero $\kappa$ [4, 8] and thus as well for a non-Maxwellian bulk distribution, with $T$ formally defined as $(m_e/n) \int v^2 \hat{f}(v) \, dv$. Here $n = \int \hat{f}(v) \, dv$ is the density unperturbed by the waves, and $\hat{f}$ is the zeroth-order (in the field amplitude) distribution function, which for linear waves equals the average of the true distribution $f(x, v, t)$; e.g., $\hat{f}(v) = L^{-1} \int f(x, v, t) \, dx$, where $L$ is the plasma length.

For slow compression, the bulk plasma remains approximately homogeneous, with the density scaling like $n \propto \mathscr{V}^{-1}$, where $\mathscr{V}$ is the plasma volume. Since $\omega_p \propto n^{1/2}$, one thereby gets $\omega_p \propto \varepsilon^{-1/2}$ for 1D compression assumed below, where $\varepsilon \equiv L/L_0$, $L$ is the plasma length, and the subscript 0 is henceforth used to indicate an initial condition. From (2.1), the wave phase velocity $v_p = \omega/k$ is given by

$$v_p = v_{p0} h(\varepsilon) \varepsilon^{1/2}, \tag{2.2}$$

where $h(\varepsilon)$ is a factor close to one and is found as follows. Since the compression is slow, the adiabatic invariant

$$vL = \text{inv} \tag{2.3}$$

is conserved for each electron. Thus, the bulk electron distribution evolves self-similarly, and the thermal velocity obeys the scaling $v_T \propto \varepsilon^{-1}$. Since $k \propto \varepsilon^{-1}$ as well, one obtains $\kappa = \kappa_0 \varepsilon^{-3/2}$; then, from (2.1) and (2.2), one finds

$$h = 1 + \frac{3}{2} \kappa_0^2 \varepsilon^{-3}. \tag{2.4}$$

Under the assumption of $\kappa \ll 1$, when (2.1), (2.2), and (2.4) are valid, the Langmuir wave growth rate, $\gamma$, is of the same sign as $v_p f'(v = v_p)$ [7]. In Maxwellian plasma, $\gamma < 0$, yielding damping. However, in the presence of a bump-on-tail distribution, an instability develops for waves with $v_p$ in the interval where $v_p f'(v = v_p) > 0$. The quasilinear theory predicts that $f$ be flattened eventually within this interval (i.e., $f'$ becomes zero), which is how the BoTI saturates. At compression, though, $v_p/v_T$ decreases as $\varepsilon^{3/2}$. Hence, modes that were initially unstable eventually become stable and experience damping, as their $v_p$ move into the region of negative $v_p f'(v = v_p)$. Notice that the *shape* of the mode spectrum also evolves through compression [5]. First of all, modes with larger $k$ have smaller $v_p \approx \omega_p/k$ and thus interact

with a larger number of resonant electrons and damp sooner. In addition, multiple excited modes whose individual trapping regions [9] formally overlap (in the sense of Refs. [10, 11]) can exchange energy through the stochastic exchange of resonant electrons [5]. For a mode with wavenumber $k$, the characteristic trapping width in velocity space is defined as

$$\delta v_k = 2\sqrt{qE_k/m_e k}, \tag{2.5}$$

where $q$ is the electron charge, and $E_k$ is the mode amplitude of the electric field [7]. The stochastic exchange of energy between modes with overlapping trapping regions results in another damping mechanism for excited waves [5]. Specifically, a mode that has become resonant with the bulk distribution and has begun damping can act as an energy sink for other modes stochastically exchanging energy with the damped mode, even if the other modes do not experience *linear* damping themselves.

## 3. Particle-in-cell simulations

In order to support the above predictions numerically, we developed an electrostatic PIC code that models plasma compression in a 1D box with the right wall at $x = L(t)$, moving with velocity $\dot{L} = V < 0$, and the left wall kept fixed at $x = 0$. To produce BoTI, electrons are initialized randomly in a homogeneous Maxwellian distribution, $f_{M1}(v)$, superposed with a much smaller, homogeneous, and symmetrically shifted Maxwellian bump, $f_{M2}(v)$. The total initial distribution function $f_0(v)$ then can be written as

$$f_0(v) = n_0 \left\{ (1 - 2\xi) f_{M1}(v) + \xi \left[ f_{M2}(v + \Delta v) + f_{M2}(v - \Delta v) \right] \right\}, \tag{3.1}$$

where $n_0$ is the bulk number density, $\xi \ll 1$ is the perturbation density, $f_{Mj}(v) = \exp(-v^2/2v_{Tj}^2)/\sqrt{2\pi}v_{Tj}$ for $j = 1, 2$; also, $v_{Tj}$ are the corresponding thermal velocities. Hard-wall boundary conditions are assumed, and total charge neutrality is maintained; hence, only standing waves with integer $m \equiv kL/(2\pi)$ can be excited. Ions are treated as a uniform charge-neutralizing background, which is a valid model under the assumption that the compression scenario is chosen appropriately [5]. The right wall is accelerated from rest to its peak velocity, coasts at constant velocity until a desired level of compression is reached, and, finally, is decelerated until the wall is at rest once again. In some simulations, the electrostatic forces were turned off in order to compare the compression of the BoTI-unstable plasma with that of a wave-free neutral gas.

The PIC code reproduces the life cycle of BoTI numerically, as illustrated in Figs. 1 and 2 using a representative set of initial parameters, namely, $\xi = 0.01$, $v_{T1} = 1.5 \times 10^9$ cm s$^{-1}$, $v_{T2} = 0.75\,v_{T1}$, $\Delta v = 5.0\,v_{T1}$, $\omega_p = 10^{11}$ s$^{-1}$, $L_0 = 2.0$ cm, and the peak wall velocity, $V = -0.067\,v_{T1}$, with the negative sign indicating compression by the right wall. Initially, the wall is at rest for 50 plasma cycles while the instability saturates (Fig. 1(c)). The wall then accelerates to its peak velocity during a single plasma cycle $\tau_{p0} = 2\pi/\omega_{p0}$ and coasts until $\varepsilon \approx 0.15$. Then the wall slows to a halt in one more plasma cycle $\tau_{p0}$, and the plasma is simulated for an additional 50 cycles at full compression. Figure 1(b) reveals that modes with $3 \lesssim m \lesssim 7$ are most strongly excited by the instability. As predicted, modes with larger $m$ damp earlier due to their smaller phase velocities and earlier transition to resonance with bulk electrons during compression. Note that the excited wave amplitudes in this case are
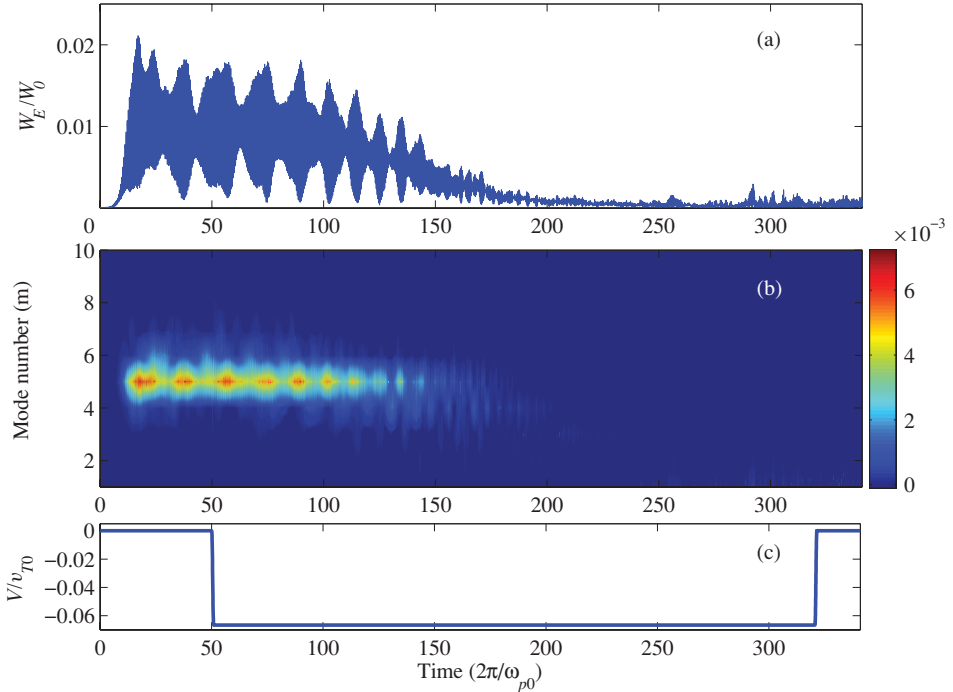
**Figure 1.** (Color online) Life cycle of bump-on-tail instability. (a) Total electrostatic energy $W_E$ normalized to total initial plasma energy $W_0$ (kinetic + electrostatic); (b) energy spectrum across lowest Fourier modes, with mode number defined as $m = k_m L/2\pi$ and same normalization as in (a); (c) wall velocity normalized to initial electron thermal velocity $v_{T0}$, with negative velocity indicative of compression.

small enough to keep the wave dynamics essentially linear; increasing the strength of the instability leads to the formation of highly nonlinear trapped particle modes, of which the governing physics will be the topic of future publications.

A more detailed view of the evolution of the electron distribution is given in Fig. 2. At $t = 0$, the weak bump is evident at suprathermal velocities, and no waves are present above the negligible initial noise level. After 10 cycles, the instability has begun to develop and modes four, five, and six (i.e., those with $m = 4, 5, 6$) can be seen growing. The modes with $m = 2, 3, \ldots, 15$ are plotted according to the mode phase velocities, which decrease with increasing $m$, while the phase velocity of the mode with $m = 1$ was too large to plot on the same figure. The height of the red bars corresponding to individual modes represents the electrostatic energy of those modes averaged over a plasma cycle, while the horizontal bars denote the width of each mode's trapping region, cf. Eq. (2.5). Modes 4–6 are found in the center of the instability domain, and by $t = 50\,\tau_{p0}$ they have saturated such that their trapping regions are confined to the velocity range where $\hat{f}(v)$ is flat. In addition, individual trapping regions overlap (again, in the sense of Refs. [10, 11]), and the electrostatic energy of each individual mode was observed fluctuating due to the stochastic exchange of energy between the modes, as discussed above. Compression begins at $t = 50\,\tau_{p0}$, and the proceeding images show each mode losing energy as the
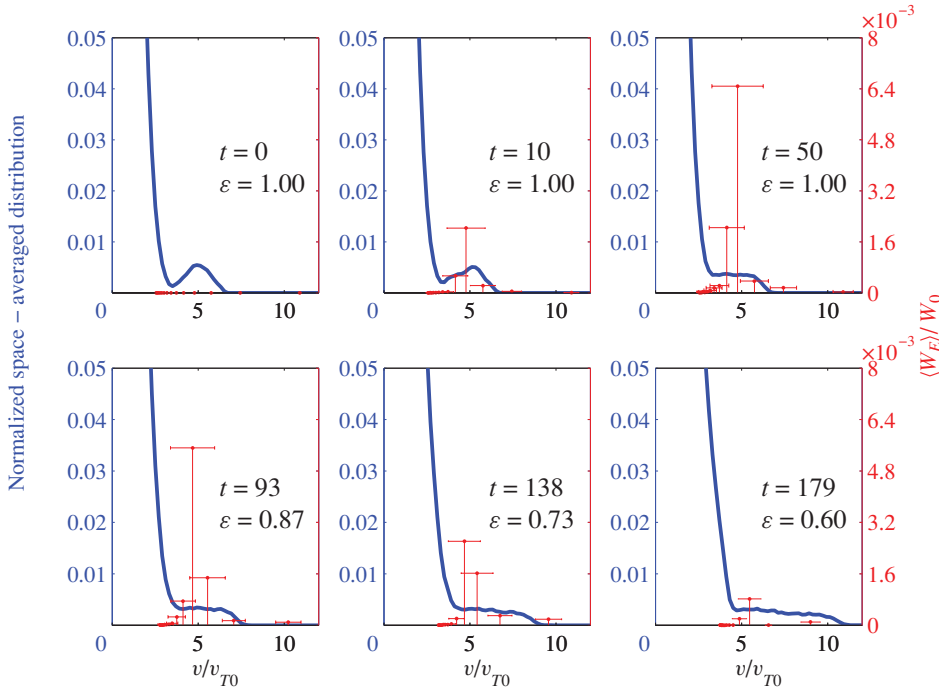
**Figure 2.** (Color online) Snapshots of the space-averaged distribution function $\hat{f}(v)$ (blue; left axes) along with the phase velocities and cycle-averaged electrostatic energies $\langle W_E \rangle$ of excited resonant modes (vertical lines, red; right axes). The horizontal bars denote the width of each mode's trapping region, $\delta v_k$ (2.5). Time $t$ is given in units of $\tau_{p0} = 2\pi/\omega_{p0}$. Compression begins at $t = 50\tau_{p0}$. The bulk distribution remains essentially Maxwellian and thus is not shown in the figure.

distribution is heated adiabatically, with the slowest modes damping away first. By $t = 179\,\tau_{p0}$, the wave energy is almost completely damped. The suprathermal tail is both flattened and broadened by the damping waves, and at later times than those shown, the flat-tail distribution continues to grow self-similarly with compression because of the conservation of the adiabatic invariant (2.3). Like in Ref. [5], the bulk distribution remains essentially Maxwellian with bulk temperature and pressure growing adiabatically, and thus it is not shown in the figure.

## 4. Energy is not a state variable

Consider the plasma total energy $W$ as the sum of the wave energy $W_w$ and the thermal energy $W_T$, for which there is a unique decomposition $W = W_w + W_T$ [12]. Although BoTI itself cannot change $W$, it does change the instantaneous ratio $\rho \equiv W_w/W = 1 - W_T/W$, as illustrated in Fig. 3. Remarkably, this affects the plasma pressure [13], defined as usual through $\mathscr{P} = -dW/d\mathscr{V}$ for adiabatic compression, and also the energy gain $\Delta W$ through compression. Specifically, for an adiabatic process, one has $W_w \propto \mathscr{V}^{-1/2}$ and $W_T \propto \mathscr{V}^{-2}$ [4, 5]. Hence, $dW_w = -W_w\,d\mathscr{V}/(2\mathscr{V})$, $dW_T = -2W_T\,d\mathscr{V}/\mathscr{V}$, and

$$\mathscr{P} = 2w(1 - 3\rho/4), \tag{4.1}$$
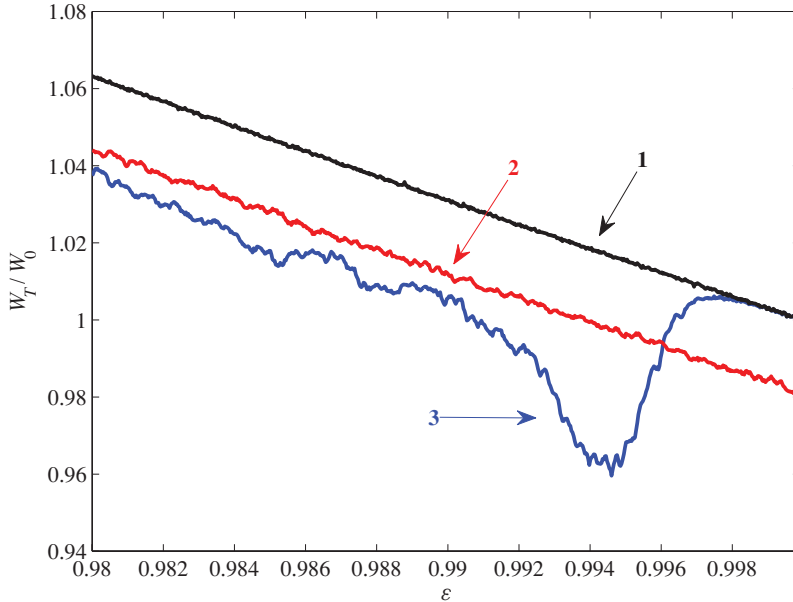
**Figure 3.** (Color online) Thermal energy $W_T$ normalized to initial total energy $W_0$ vs. $\varepsilon \equiv L/L_0$ for three different compression scenarios: (1) neutral gas without BoTI; (2) plasma compression delayed $50\tau_{p0}$ while instability saturates; and (3) plasma compression begins immediately. The drop in $W_T$ in the plasma systems relative to the neutral gas corresponds to a decrease in plasma pressure $\mathscr{P}$ (4.1), meaning less work is required to compress the plasma compared to the neutral gas (4.2). Parameters same as in Figs 1 and 2, except $\xi = 0.025$ and peak wall velocity $V = -0.013v_{T1}$. Note that the initial stage corresponds to the right of the figure, where $\varepsilon = 1$, and the final stage is to the left, where $\varepsilon < 1$.

where $w \equiv W/\mathscr{V}$ is the average density of the total energy. Since BoTI does not affect $w$ but increases $\rho$ (at least temporarily), it thereby decreases $\mathscr{P}$. Equivalently, the BoTI increases the plasma compressibility [14], given by $\beta \equiv -(1/\mathscr{V})d\mathscr{V}/d\mathscr{P}$, or $\beta = 1/\mathscr{P}$ here. Thus, the total energy gain $\Delta W = \int \dot{W}\, dt$ is decreased, since

$$\dot{W} = 2W\left[1 - 3\rho(t)/4\right]\eta(t), \qquad (4.2)$$

where the compression rate $\eta \equiv -\dot{\mathscr{V}}/\mathscr{V}$ has been introduced. The function $\rho(t)$ can vary depending on the manner in which BoTI developed during compression. Therefore, $W$ is *not* a function of the plasma volume and, in this sense, is not a state variable, unlike for a neutral gas or a plasma containing only cold and undamped waves [4, 5].

These predictions are supported by our numerical simulations, as seen in Table 1. The first set of parameters in Table 1 corresponds to Fig. 3; others show even wider variation between compression scenarios. In every compression scenario, the presence of resonant waves leads to a lower final energy than the corresponding neutral gas. Specifically, a scenario resulting in a larger decrease in $W_T$ during compression, observed in Fig. 3, correctly leads to a smaller final energy once all of the waves are fully damped (4.2). This confirms our prediction that transforming kinetic energy into the energy of Langmuir waves reduces the amount of mechanical work needed to compress a plasma down to a specified size.

**Table 1.** Final energies under nine different compression scenarios with identical initial conditions. The final stage of the compression corresponds to $\varepsilon = 0.15$, by which time all waves are fully damped. The first column shows the peak wall speed. The second column shows the delay time (in units $\tau_{p0}$) prior to compression (cf. Fig. 1(c)). The third column shows the total energy of the plasma final state, $W_f$, normalized to $W_0$. The fourth column shows, for reference, the same $W_f$ normalized to the final energy of a neutral gas, $W_{f,g}$, compressed similarly but without BoTI.

| $V/v_{T1}$ | Delay ($\tau_{p0}$) | $W_f/W_0$ | $W_f/W_{f,g}$ |
|---|---|---|---|
| 0.013 | 50 | 46.955 | 0.9937 |
| | 0 | 46.843 | 0.9914 |
| 0.067 | 50 | 46.895 | 0.9860 |
| | 0 | 46.760 | 0.9832 |
| 0.333 | 50 | 46.953 | 0.9439 |
| | 0 | 46.497 | 0.9348 |

## 5. Discussion

There is an interesting comparison to be made with other variations on BoTI. The time-dependency of the compression for BoTI in compressing plasma removes constraints on the available time-asymptotic solution, similar to the case of multiple bumps-on-tail in the non-compressing plasma. For a non-compressing plasma, BoTI have a time-asymptotic solution in which the bump flattens into the so-called *quasilinear plateau* [6], and the energy converted to electrostatic waves is insensitive to the details of the instability evolution. The time-asymptotic electron distribution in the resonant region must be flat; otherwise, the instability could develop further. Hence, the free energy available in the resonant region for conversion to electrostatic wave energy is uniquely determined, at least for the *one* bump-on-tail distribution function. For multiple bumps on the tail of the distribution function, no such unique time-aymptotic distribution occurs [15]. In the case of multiple bumps, each bump flattens separately due to quasilinear relaxation, but the order in which the bumps flatten, which can be sensitive to the details of the initial wave energy spectrum, determines the final height of each bump. Thus, the free energy available in the resonant region for conversion to electrostatic wave energy is not uniquely determined for multiple bumps on the tail.

One can also compare the free energy available through diffusion of resonant electrons with the theoretically maximum free energy available by evolution of the Vlasov equation, namely the free energy available under the so-called *Gardner restacking* [16, 17], in which the electron distribution function is constrained only by phase space conservation in configuration-velocity space, $f(x, v)$. However, in slowly compressing plasma, the Gardner free energy would remain insensitive to the details of the compression; clearly, since each phase space element would retain its ordering under the compressing transformation $f(v) \rightarrow af(av)$. Thus, restacking prior to compression or subsequent to compression yields the same final distribution and frees up the same amount of particle energy. However, the Gardner free energy is not generally of practical importance, since waves generally act diffusively in wave–particle interactions in plasma. The free energy available under the diffusive constraint, namely through the quasilinear relaxation of the distribution function

in the resonant regions, is of practical interest, for example, in the case of α-channeling, where the particle free energy is liberated to produce wave energy that in turn can perform other useful purposes (like ion heating or current generation) [18].

Thus, whether in the case of multiple bumps-on-tail in non-compressing plasma, or one bump-on-tail in compressing plasma, the free energy available through wave–particle diffusion is no longer uniquely determined just from the initial particle distribution, and therefore other arrangements must be made for the maximum release of this energy. Moreover, although we considered here only compression of the one bump-on-tail distribution, clearly more flexibilities in the final state would result in the event of compressing a plasma with multiple bumps-on-tail. In addition to the energy in the final state varying with the details of the compression history, it can be imagined that there can now be several abrupt changes in pressure as waves are damped in different resonant regions.

The mechanical compression by moving hard walls modeled in the PIC code serves as a simple, albeit idealized, means to produce compression of the bulk plasma in order to demonstrate the desired effects. However, a practical implementation of the analysis presented here should not be restricted only to literal realizations of this compression scheme. For instance, compression may be produced by appropriately chosen bulk plasma drift motion, as with the ballistic compression of space-charge waves in velocity-chirped beams [19], or by the presence of a spatiotemporally-varying magnetic field, to name two examples. As the compression scenario changes, so might the types of waves present in the system also change. Yet, in any case, the basic small-wave analysis presented here, as a first approximation of the associated wave phenomenology, should be qualitatively unchanged.

Note that the considerations here of BoTI are entirely in 1D, where the compression takes place parallel to the wave phase velocity and parallel to the velocity direction where there is a bump-on-tail. Many of the considerations here, however, can be expected to pertain, albeit with modification, to the case of compression perpendicular to the wave phase velocity, where the compression similarly increases the wave energy and changes the wave phase velocity [4, 5]. In particular, it can be expected that, for perpendicular compression, the time-asymptotic electron velocity distribution would also be dependent on the time history of the compression. However, for perpendicular compression, the phase velocity of the plasma waves increases rather than decreases with compression, since the wavenumber is left unchanged by the compression, but the plasma frequency increases with density. Thus, there is the opportunity to draw out a longer tail in the final electron distribution function, since the larger velocity plasma waves would damp on the tail of the distribution function rather than on the bulk of the distribution function as in the case considered here.

Moreover, in the case of compression in the perpendicular direction, there is the opportunity for the plasma to carry current in the event that the initial distribution function is asymmetric in velocity space, namely when the initial bump-on-tail occurs only for electrons traveling in one direction. Under 1D compression, in which all particles are reflected at the boundaries, this asymmetry would vanish quickly. However, in the case of compression perpendicular to the direction of the wave vector of the excited mode, with periodic boundary conditions in the parallel

direction (the direction of the asymmetry), this asymmetry in the parallel direction would persist. This means that not only can the amplified waves drive electric current and thereby generate magnetic fields, but the current drive in the final state can be particularly efficient, since high-phase velocity waves tend to exhibit a very efficient current drive effect [20]. Note that in the example envisioned here, the total electron current is not enhanced by the compression, since the waves carry no momentum; however, electron–ion collisions would quickly convert the skewness in the electron velocity distribution to net current as the bulk electron current dissipates while the current carried by the relatively collisionless tail persists, like in other current drive schemes involving fast electrons.

## 6. Conclusions

Simulations of BoTI for plasmas subject to 1D mechanical compression show that the exact nature of the final state depends on the compression scenario; namely, multiple final energy states can be accessed under different scenarios, unlike for stationary medium. The transformation of thermal energy into wave energy increases the plasma compressibility, thereby decreasing the amount of mechanical work required to compress the plasma. Also, the energy spectrum of the excited modes can be tailored by choosing a particular compression rate as a function of time, offering a new technique for manipulating plasmas.

## References

[1] Moses, E. I. 2009 *Nucl. Fusion* **49**, 104022.

[2] Kirkpatrick, R. C., Lindemuth, I. R. and Ward, M. S. 1995 *Fusion Tech.* **27**, 201.

[3] Ryutov, D. D., Derzon, M. S. and Matzen, M. K. 2000 *Rev. Mod. Phys.* **72**, 167.

[4] Dodin, I. Y., Geyko, V. I. and Fisch, N. J. 2009 *Phys. Plasmas* **16**, 112101; see also refs. therein.

[5] Schmit, P. F., Dodin, I. Y. and Fisch, N. J. 2010 *Phys. Rev. Lett.* **105**, 175003.

[6] Krall, N. A. and Trivelpiece, A. W. 1973 *Principles of Plasma Physics*, Chap 10. Columbus, OH: McGraw-Hill.

[7] Stix, T. H. 1992 *Waves in Plasmas*, Chap. 8 and Secs. 7.7, 7.8. New York, NY: AIP.

[8] Tokatly, I. and Pankratov, O. 1999 *Phys. Rev.* B **60**, 15550.

[9] T. O'Neil 1965 *Phys. Fluids* **8**, 2255.

[10] Chirikov, B. V. 1979 *Phys. Rep.* **52**, 263.

[11] Escande, D. F. 1982 *Phys. Scr.* **T2**, 126.

[12] Dodin, I. Y. and Fisch, N. J. 2010 *Phys. Lett.* A **374**, 3472.

[13] Kentwell, G. W. and Jones, D. A. 1987 *Phys. Rep.* **145**, 319.

[14] Reif, F. 1965 *Fundamentals of Statistical and Thermal Physics*, Secs. 5–7. Columbus, OH: McGraw-Hill.

[15] Fisch, N. J. and Rax, J. M. 1993 *Phys. Fluids* B **5**, 1754.
[16] Gardner, C. S. 1963 *Phys. Fluids* **6**, 839.
[17] Dodin, I. Y. and Fisch, N. J. 2005 *Phys. Lett*. A **341**, 187.
[18] Fisch, N. J. and Rax, J. M. 1992 *Phys. Rev. Lett*. **69**, 612.
[19] Stepanov, N. S. 1963 *Izv. Vyssh. Uchebn. Zaved. Radiofiz*. **6**, 112.
[20] Fisch, N. J. 1987 *Rev. Mod. Phys*. **59**, 175.